International Journal of Basic and Applied Sciences, 14 (8) (2025) 142-153

International Journal of Basic and Applied Sciences

Website: www.sciencepubco.com/index.php/IJBAS
https://doi.org/10.14419/9beq9v16
Research paper

Material Synergy and Efficiency Enhancement in Axial Flux PMSM: Influence of Magnet, Core and Conductor Combinations

Sandhiya Swaminathan *, Saravanan Sivasamy, Srinivas K. N.

SRM Institute of Science and Technology, Ramapuram, Chennai, India
**Corresponding author E-mail: ss9597@srmist.edu.in*

Received: November 7, 2025, Accepted: December 3, 2025, Published: December 7, 2025

Abstract

This study investigates the material-dependent performance of an axial flux permanent magnet synchronous motor (AF-PMSM) through a systematic evaluation of magnet, core, and conductor combinations. The analysis reveals that transitioning from ferrite to high-energy NdFeB magnets significantly enhances efficiency, ranging from 74.58% to 85.91%, while concurrently increasing sensitivity to iron-core losses. Employing low-loss core materials, particularly Hiperco50, markedly improves overall efficiency, underscoring the necessity of advanced magnetic alloys in high-flux-density motor systems. Among the examined magnets, the advanced N55 grade NdFeB achieves the highest efficiency (87.19%) and lowest loss, surpassing Alnico5 and SmCo24. Although SmCo24 offers superior thermal stability, its per-formance remains inferior to that of N55. Conductor analysis further reveals that silver windings yield the highest efficiency (88.03%) and lowest total losses, slightly outperforming conventional copper at the expense of increased weight. Gold and aluminium conductors, by contrast, exhibit reduced efficiency due to higher resistivity. The findings highlight the crucial interplay between magnet strength, core loss characteristics, and conductor resistivity in determining overall AF-PMSM efficiency, providing valuable insight for the material optimiza-tion of traction motors in electric vehicle applications.

Keywords: *Axial Flux Permanent Magnet Synchronous Motor (AF-PMSM); Material Optimization; Motor Efficiency; Electric Vehicle Traction Drive.*

1. Introduction

The worldwide shift toward low-carbon transportation has significantly boosted electric vehicle (EV) adoption, where the traction motor plays a crucial role in determining overall efficiency, power density, and sustainability. Permanent Magnet Synchronous Motors (PMSMs) have become the dominant propulsion choice in EVs due to their high energy efficiency typically between 92% and 97%, compact size, and excellent torque capabilities. PMSMs differ from conventional induction motors by embedding permanent magnets in the rotor, which eliminate the need for rotor windings and reduce associated losses. This design advantage leads to higher power density, lighter motor weight, and greater reliability essential for traction applications [1] [2].

Recent advancements in high-silicon electrical steels and nanocrystalline alloys have shown promising reductions in core losses and im-proved thermal stability in PMSM stator cores, as reported in Journal of Magnetism and Magnetic Materials[3].Soft magnetic composites (SMCs) with nanostructured microstructures facilitate three-dimensional magnetic flux conduction, offering enhanced efficiency and ena-bling flexible axial flux motor designs [4].

Selecting appropriate materials is key to optimizing efficiency and power density in these compact motor designs. For EV-grade PMSMs, it is important to balance efficiency, cost, thermal resistance, and weight. Rare-earth permanent magnets along with advanced magnetic alloys support efficiencies above 95%, thereby improving driving range and battery lifespan. Thermal management is critical since EV motors often operate at elevated temperatures (150–200°C), necessitating materials and design solutions that maintain performance under these conditions. Additionally, lightweight materials and innovative conductor and magnet configurations help boost torque density while keeping overall system weight low [2] [5]. Additive manufacturing techniques have been experimentally validated for fabricating complex rotor and stator geometries with integrated cooling channels, resulting in improved power density and enhanced heat dissipation in axial flux PMSMs [6]. Comprehensive multiphysics simulations that couple electromagnetic, thermal, and mechanical stresses are critical to predicting motor reliability and performance under real EV operating conditions [7].

PMSMs outperform other electric motor types such as induction motors, switched reluctance motors, and synchronous reluctance motors in torque output and power density for the same volume [8]. This results in better acceleration, improved efficiency, and easier integration into compact EV drivetrains. However, the dependence on rare-earth elements like neodymium and dysprosium introduces challenges including high costs, supply chain vulnerabilities, and environmental impacts related to mining and processing. These include habitat disruption, generation of toxic byproducts, and significant carbon emissions. Furthermore, rare-earth resources are concentrated

geographically, leading to supply and price instability, which drives research toward more sustainable alternatives [9] [10]. Optimization of fractional-slot concentrated winding (FSCW) configurations combined with innovative cooling strategies significantly reduces winding copper losses and core heating in axial flux PMSMs, enhancing continuous power rating [11].

Recent research has focused on rare-earth-free motor technologies, especially Axial Flux Permanent Magnet Synchronous Motors (AF-PMSMs). Compared to traditional radial-flux motors, AF-PMSMs offer advantages like higher power density, shorter end windings, and improved cooling features, making them highly desirable for EVs . Their design flexibility allows use of ferrite or other non-rare-earth magnets without compromising electromagnetic performance. While ferrite magnets have lower magnetic energy density than NdFeB magnets, design enhancements such as flux-focusing rotors, fractional-slot concentrated windings, and advanced control strategies help address this limitation. Accurate modeling through finite element analysis (FEA) supports optimization of electromagnetic and thermal behavior in these rare-earth-free motors [12 - 14] [6].

Various studies investigate new modeling techniques, materials, and structures for sustainable PMSMs. Traditional PMSMs rely heavily on NdFeB magnets, raising concerns about supply risks and environmental costs, which are prompting the exploration of rare-earth-free designs [15]. A 3-D nonlinear magnetic equivalent circuit model has been proposed for wound-rotor synchronous machines that efficiently accounts for leakage flux and axial field effects with less computation than full 3-D FEA [16]. An approximate multi-layered model has been developed to reduce AF-PMSM complexity by relating it to radial-flux equivalents [17]. Genetic algorithms have been applied to optimize a TORUS-type double-rotor AF-PMSM, achieving higher torque density and efficiency suited for EV use [18].

On the materials front, Metal Amorphous Nanocomposites (MANCs) have demonstrated their ability to reduce iron losses while achieving high saturation magnetization. A prototype flux-switching motor reached over 6 kW/kg in specific power and almost 99% efficiency, rivaling rare-earth [19]. Soft magnetic composites (SMCs) have shown production cost reductions of 16–29% and life-cycle carbon emissions lowered by 21–38%, without loss of performance [20]. Rare-earth-reduced multilayer interior PMSMs with double-layer U-shaped rotors have improved efficiency and reduced cogging torque [21]. Flux barrier placement optimization in synchronous reluctance motors has cut torque ripple by over 50% and increased average torque by 13% [22]. he scalability of ferrite-based bi-axial excitation synchronous machines from small prototypes to 100 kW traction motors suitable for EVs has been experimentally confirmed [23].

Third-harmonic current injection reduces iron losses in rare-earth-free PMSMs and complements material and rotor developments [24]. Environmental impacts of rare-earth extraction, including waste and emissions, have been highlighted in the study [15] . Ferrite- and SMC-based motors significantly cut carbon footprints compared to NdFeB-based systems [20]. MANC-based AF-PMSMs have been shown to lower operational energy consumption, and reluctance machines eliminate environmental issues related to permanent magnets [19].

Although rare-earth-free motors currently offer somewhat lower torque density, they provide substantial advantages in recyclability, sustainability, and supply security. Despite significant progress in AF-PMSM topologies and advanced magnetic materials, a clear quantitative framework linking material choices (core, magnet, and conductor) to electromagnetic performance and efficiency in rare-earth-free AF-PMSMs for EVs is still missing. This work specifically addresses this problem by designing and numerically analysing an EV-grade AF-PMSM while systematically varying core materials, permanent magnet grades, and conductor options to evaluate their impact on torque production, losses, efficiency.

2. Motor Design

The single-rotor single-stator AF-PMSM model was created and analyzed using finite element analysis (FEA) to evaluate the electromagnetic performance of a rare-earth-free design capable of delivering 2.5 kW power, 6.1 Nm torque, and operating at a speed of 3900 rpm, suitable for electric vehicle applications. The aim is to assess the electromagnetic performance of a rare-earth-free design with enough torque density for EV applications.

2.1. Stator design

The stator is wound with 12 poles and 15 slots utilizing a fractional slot concentrated winding (FSCW) termination in a three-phase star formation. The laminated stator core was designed using Steel_1010 material from the library, it has a stacking factor of 0.95. The stator details are presented in Table I. Figure 1 represents the 2D geometry of the stator core of the targeted AF-PMSM. The stator core has the magnetic flux paths that are optimized to reduce the magnetic reluctance and effectively use the active material.

Table 1: Stator Design Parameters of AF-PMSM

Parameter	Value
Number of Poles	12
Number of Slots	15
Winding Connection	3-phase star
Outer Diameter	120mm
Inner Diameter	70mm
Core Length	25mm
Stacking factor	0.95mm
Slot type	Trapezoidal
Core type	Steel_1010
Hs0	1.5mm
Hs1	2mm
Hs2	13mm
Bs0	3mm
Bs1	8mm
Bs2	8mm
Rs	0.4mm

The geometry also guarantees enough structural strength combined with downsizing, which is important for the lightweight EV traction motor. Figure 2 presents stator slot geometry in which slot shape and dimensions are carefully designed so that required space for full insertion of the windings is satisfied, keeping high mechanical strength of the stator core as well. The slot structure also results in improved

thermal shedding, reduced eddy current and increased filling factor. Reasonable slot design is of great importance for AF-PMSMs, as it is directly related to the flux distribution and electromagnetic characteristics.

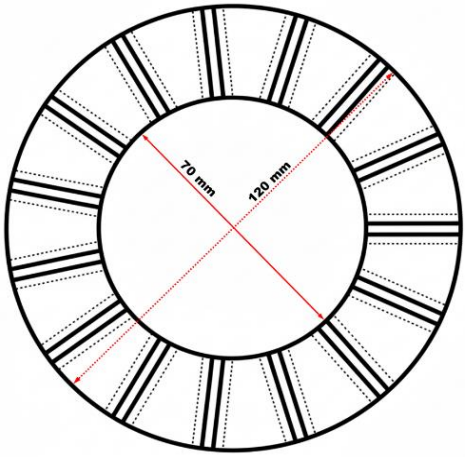

Fig. 1: Stator Design Parameters of AF-PMSM.

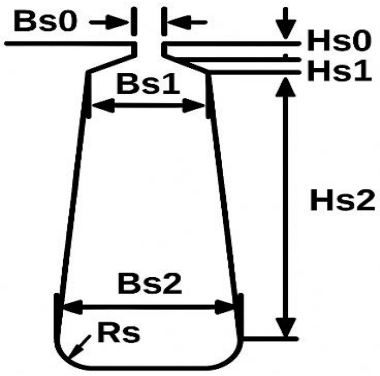

Fig. 2: Stator Slot Geometry Detailing Slot Shape and Dimensions.

2.2. Winding configuration

The stator winding employs two layers with half-coiled conductors, made of copper. Each slot accommodates 48 conductors with one parallel branch. The winding specifications are listed in Table II. Figure 3 depicts the winding arrangement of the AF-PMSM. A fractional-slot concentrated winding (FSCW) configuration has been adopted instead of a distributed scheme. This winding topology reduces the end-winding length, thereby lowering copper losses and improving the overall power density of the motor. Additionally, concentrated windings facilitate modular coil construction and simplify the manufacturing process, which is advantageous for axial flux machines. Although FSCW introduces higher harmonic content in the air-gap flux compared to distributed windings, proper slot/pole selection (15 slots and 12 poles in this design) mitigates excessive harmonic torque ripple while ensuring compactness, higher efficiency, and ease of cooling integration.

Table 2: Stator Design Parameters of AF-PMSM

Parameter	Value
Number of layers	2
Type	Half- coiled
Parallel Branches	1
Conductor per slot	48
Coil pitch	1
Strands per conductor	1
Conductor material	Copper 75C

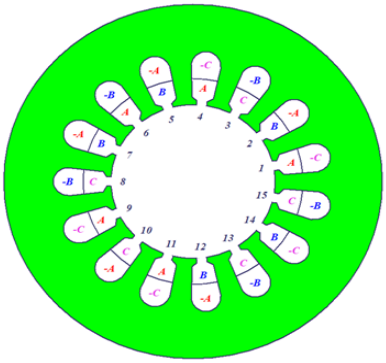

Fig. 3: Stator Winding Arrangement for Axial Flux PMSM.

2.3. Rotor design

The rotor is designed with 12 surface-mounted poles with the material Steel_1010 and with a stacking factor of 0.95. Ferrite permanent magnets, 25 mm in length and 8 mm in thickness are arranged in each pole. The magnet embrace ratio of 0.9 provides a strong magnetic coupling, ensuring maximum torque is shown in Table III.

Table 3: Rotor Specifications of Axial-Flux PMSM

Parameter	Value
Outer Diameter	120mm
Inner Diameter	70mm
Core Length	15mm
Stacking factor	0.95
Core material	Steel_1010
Magnet length	25mm
Magnet thickness	8mm
Embrace ratio	0.9

2.4. Circuit parameters

The motor drive circuit was simulated using the switching parameters like trigger pulse width (TW) of 120°, transistor drop of 0.7 V, and diode forward voltage drop of 0.7 V while mechanical losses included 12 W of friction losses as well as 12 W windage loss, both measured at a reference speed of 3000 rpm.

2.5. Geometric modelling

Figure 4 shows the 2D View of the single-stator single-rotor AF-PMSM and Figure 5 shows the 3D model of the motor. The choice of such an arrangement is made to keep the design simple while achieving high torque density. The 3D model is responsible for the axial flux topology which the magnetic flux passes in the stator-rotor interface. This can make the axial length of the motor shorter and the power ratio light, which has benefits for EV applications. The model is additionally structured such that electromagnetic, thermal, and NVH analyses can be performed for complete performance assessment in future.

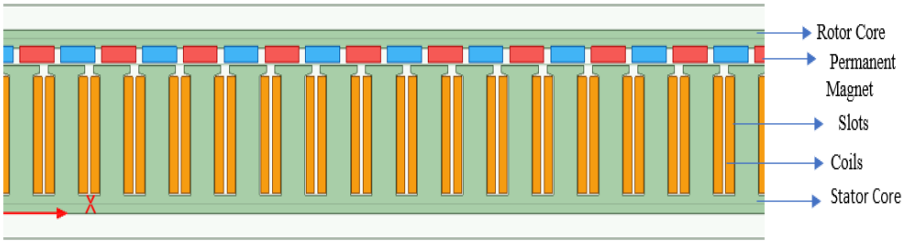

Fig. 4: 2D view of Single-Stator Single-Rotor Axial Flux PMSM.

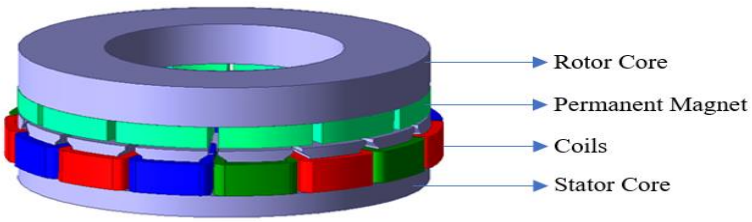

Fig. 5: 3D Model of Single-Stator Single-Rotor Axial Flux PMSM.

2.5.1. FEA procedure for electromagnetic design

Figure 6 illustrates the iterative process for electromagnetic design optimization using finite element analysis (FEA). The workflow begins with fixed independent parameters, such as output power and rated speed, and designer-adjustable variables, including magnetic loading (Bav), electric loading (ac), aspect ratio (ar), and stator winding current density (Jsw). These parameters are input into the electromagnetic design block, where direct and indirect dependent variables such as weight of active parts (KgAPs), outer stator diameter (OSD), and efficiency (Eff) are computed as functions of the input variables:

KgAPs = f (Bav, ac, Jsw,…)

OSD =f (Bav, ac, ar,…)

Eff =f (Bav, ac, Jsw,…..)

Electromagnetic performance indicators, such as output torque, are continuously evaluated, while indirect dependents are fed into the convergence logic module. This module assesses whether the calculated performance meets the specified design targets and constraints. If not, the adjustable independent variables are iteratively re-entered into the electromagnetic design block until optimized convergence is achieved. This closed-loop structure ensures a systematic and robust approach to parameter tuning, balancing electromagnetic, geometric, and performance characteristics throughout the iterative FEA design cycle.

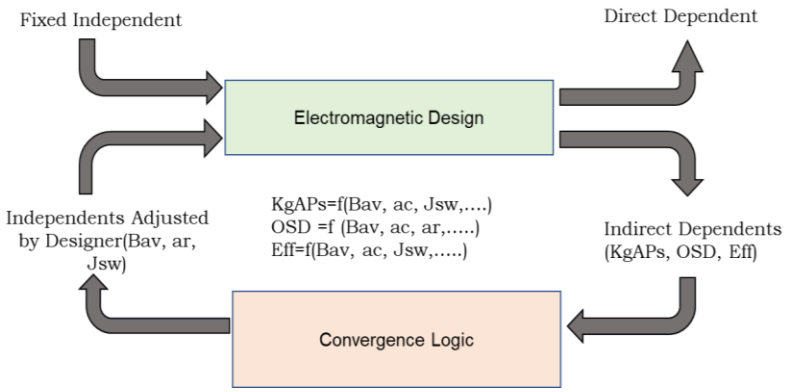

Fig. 6: FEA Procedure for Electromagnetic Design.

In addition to detailed electromagnetic design, consideration of thermal management and mechanical robustness is critical to unlock the potential of rare-earth-free AFPMSMs in the practical electric vehicle applications. Reduced magnetic energy density of ferrite and other magnets require cooling strategies to be optimised in order to manage the heat generated and allow the magnets to avoid degradation and maintain high performance. Moreover, Structural design parameters such as stacking factor, lamination-material quality, and rotor-assembly rigidity have a direct effect on the long-term durability of the motor and its noise-vibration-harshness (NVH) performance. In particular, it has been shown that the use of fractional slot concentrated windings increases electromagnetic efficiency and leads to lower end-winding length and hence reduced copper losses and better thermal dissipation paths. Such design optimizations also support modular manufacturing processes, including for cost savings, scalability, etc. In addition, through the use of multilayer axial flux architectures, more flexible magnet location and enhanced thermal management are achieved to compensate for weaker magnetic properties associated with rare-earth free materials. Taken together, these mechanical and thermal advancements enable viable performance operation consistent with the high demands of e-vehicle traction systems that match the promising environmental virtues of REF-AFPMSMs.

To verify the performance of the proposed rare-earth-free AF-PMSM design, full simulations were conducted using advanced modelling methodology including the important electromagnetic effects peculiar to the axial flux arrangement. This involved explicit treatment of the axial fringing flux and leakage paths, which are often ignored in simpler models, but have strong effects on torque generation and efficiency. The fractional slot concentrated winding topology was optimized for the trade-off between harmonic reduction and manufacturability, resulting in a small motor size that is well suited for electric vehicle packaging. The focus was also given to the magnet geometry and to the embrace ratio which further contributed to increase the performance of magnetic flux utilization even though the remanence of ferrite magnet was lower. Also, mechanical and thermal concerns, including stacking factor, lamination material choice and rotor assembly integrity, were integrated into the design to ensure the required durability and reliability for typical EV duty cycles. This multidisciplinary approach was able to reach impelling electromagnetic figures of merit and established the basis for a scalable and competitive production of environmentally friendly traction motors. These comprehensive design principles are indispensable in mitigating the inherent weaknesses of rare-earth-free materials, and in promoting the extensive application of them in high-performance electric mobility technologies.

3. Simulation Results and Analytical Calculation

The study involved both steady-state and transient electromagnetic analyses to comprehensively assess the machine's dynamic and static performance.

3.1. Steady state analysis

The steady-state performance of the designed PMSM was evaluated in terms of input current, torque, output power, and efficiency. Figure 7 shows the output power reaching approximately 4.5 kW under rated conditions. The torque waveform with a rated value of about 6.1 Nm, is shown in Figure 8. Figure 9 shows the input current which increased gradually with rotor position, indicating balanced excitation and proper magnetic field alignment. The efficiency showed a bell-shaped profile, attaining a maximum of around 61% is shown in Figure 10. These results demonstrate stable and efficient steady-state operation of the motor.

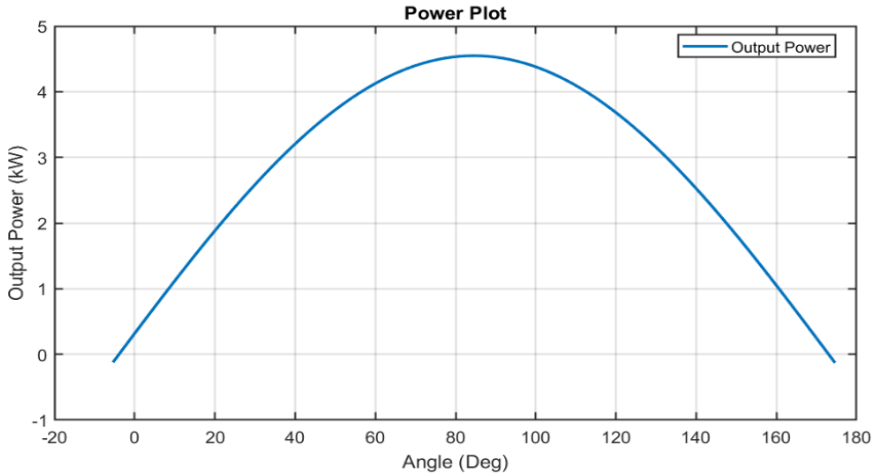

Fig. 7: Power plot of Single-Stator Single-Rotor Axial Flux PMSM.

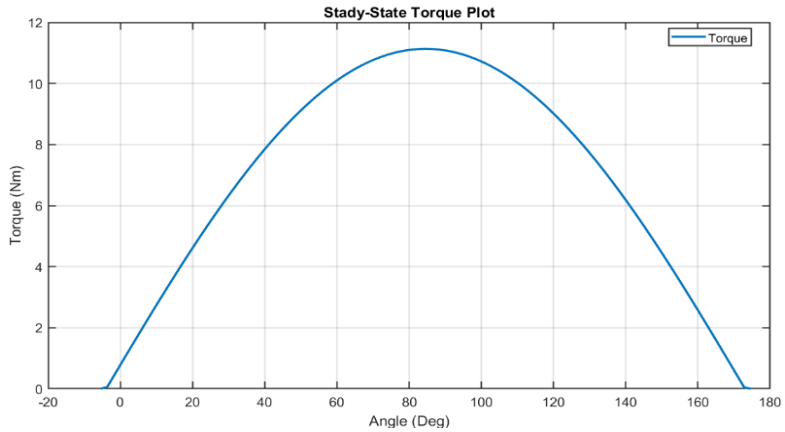

Fig. 8: Torque plot of Single-Stator Single-Rotor Axial Flux PMSM.

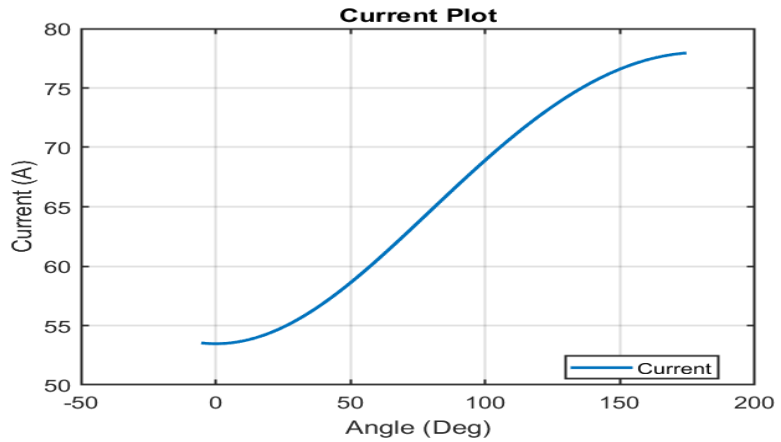

Fig. 9: Current plot of Single-Stator Single-Rotor Axial Flux PMSM.

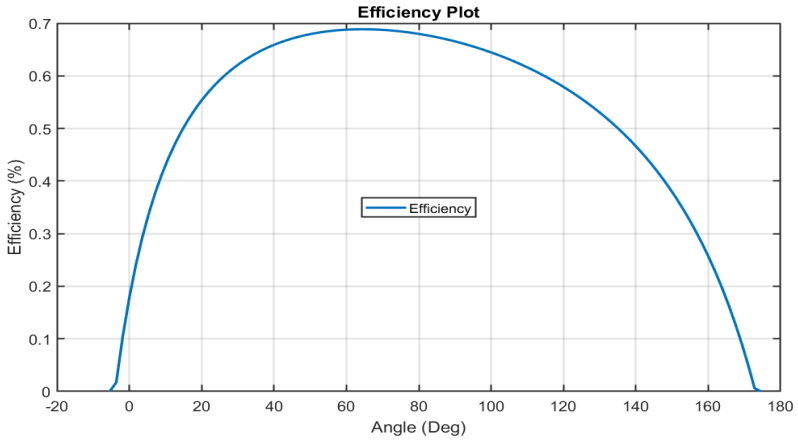

Fig. 10: Efficiency plot of Single-Stator Single-Rotor Axial Flux PMSM.

3.1.1. Inference

In order to validate the simulation proofs analytically, in this inference section the torque in Nm and the efficiency are calculated using respective formula and hence proved to match with the simulation results.
In field-oriented control (FOC), the synchronous reference frame currents (d-axis and q-axis) are transformed to three-phase stationary frame currents via the inverse Park transformation. This transformation is fundamental to understanding phase current waveforms under FOC operation.
Standard inverse Park transformation:

$$i_a = i_d \mathrm{Cos}\theta_e - i_q \sin\theta_e \quad (1)$$

$$i_b = i_d \cos(\theta_e - 120°) - i_q \sin(\theta_e - 120°) \quad (2)$$

$$i_c = i_d \cos(\theta_e - 120°) - i_q \sin(\theta_e + 120°) \quad (3)$$

Where θ_e is the electrical rotor angle and i_d, i_q are the direct and quadrature axis currents respectively. For maximum torque per ampere (MTPA) control strategy, the direct-axis current is set to zero (i_d=0) to maximize torque production from a given current magnitude. Under rated operation, the q-axis current is fixed at:

$$i_q = \frac{T_e}{\frac{3}{2}p\lambda_m} \quad (4)$$

Where Te is electromagnetic torque in Nm, p is number of pole pairs and λ_m is permanent magnet flux linkage.
Mean Radius = 0.095m
Pole pitch = 0.05m
Magnet area per pole, A = pole pitch * magnet length, A=0.00125m^2
Remanence, B_r (Ferrite) = 0.4Tesla
Magnetic Flux, $\varphi = B_r * A$
φ =0.0005Wb, Turns per phase, N=48

Permanent Magnet Flux Linkage, $\lambda_m = N * \varphi$ (5)

$\lambda_m = 0.024$Wb
Therefore, from equation 4, $i_q = 28.24$ A. With $i_d = 0$,

$$i_a = -i_q \sin\theta_e \quad (6)$$

$$i_b = -i_q \sin(\theta_e - 120°) \quad (7)$$

$$i_c = -i_q \sin(\theta_e + 120°) \quad (8)$$

This simplified form shows that all three phase currents are sinusoidal functions of the electrical rotor angle with 120° phase displacement, characteristic of balanced three-phase AC operation. From the simulation results of Figure 7 and Figure 8, it is evident that at an electrical rotor angle of $\theta_e = 30°$ (mechanical angle 5°), the motor achieves its rated power of 2.5 kW while producing the rated torque of 6.1 Nm under field-oriented control. This operating point corresponds to optimal alignment of the flux and current vectors, confirming the validity of the MTPA control strategy for efficient power conversion. This can be proved by, at angle $\theta_e = 30°$, by substituting $i_q = 28.24$ A, we get

$$i_a = -14.12 \text{ A} \quad (9)$$

$$i_b = 28.24 \text{ A} \quad (10)$$

$$i_c = -14.12 \text{ A} \quad (11)$$

To validate the inverse transformation, the forward Park transformation reconstructs the original d-q components:

$$i_d = \frac{2}{3}[i_a \cos\theta_e + i_b \cos(\theta_e - 120°) + i_c \cos(\theta_e + 120°)] \quad (12)$$

$$i_q = -\frac{2}{3}[i_a \sin\theta_e + i_b \sin(\theta_e - 120°) + i_c \sin(\theta_e + 120°)] \quad (13)$$

At $\theta_e = 30°$, $i_d = 0$A , $i_q = 28.24$A. The rated phase currents derived from the inverse Park's transformation directly produce the electromagnetic torque $T_e = 6.1$ Nm and output power, $P_{out} = T_e * \omega_r$ = 2.5 kW at 3900 rpm.

3.2. Transient analysis

The transient behavior of the AF-PMSM is crucial for evaluating its dynamic response during motor startup, load disturbances, and speed transitions conditions frequently encountered in electric vehicle operation. The transient simulation was conducted over a 15ms interval to capture the complete motor startup sequence.

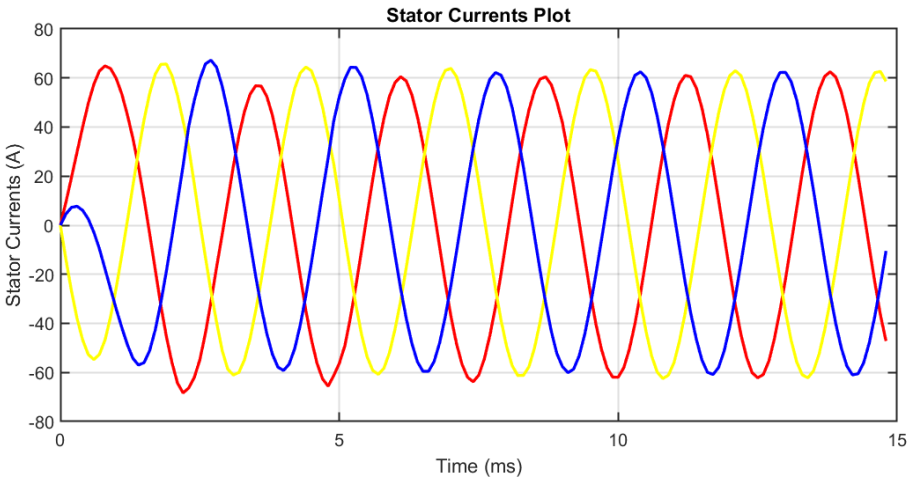

Fig. 11: Stator Current Waveforms of Phases A, B, and C Under Transient Operation.

The stator current waveforms of three phases are shown in Figure 11. The current characteristics are indicative of effective PMSM control and suggest that the excitation conditions are ideal for generating smooth rotating magnetic fields within the stator. The amplitude of each phase current appears symmetrical, with peak values approaching ±70 A, and periodicity maintained consistently throughout the observed window.

Figure 12 shows the d-axis and q-axis inductances (Ld and Lq) over a transient simulation. The initial variations observed in both inductance profiles are associated with the motor's transient behavior during the startup phase. As the simulation progresses, the values of L_d and L_q become steady, signifying that the machine has reached a stable operating condition. The d-axis inductance (L_d), illustrated by the blue curve, consistently remains lower than the q-axis inductance (Lq), shown in red. This condition, where $L_q > L_d$, is characteristic of salient-pole PMSM configurations and contributes to the production of additional reluctance torque, thereby improving the overall torque capability. The minimal deviation between L_d and L_q further indicates low magnetic saturation and a well-balanced flux linkage distribution across the stator and rotor. Consequently, the designed AF-PMSM demonstrates a stable electromagnetic response, ensuring high torque efficiency and reliable dynamic performance.

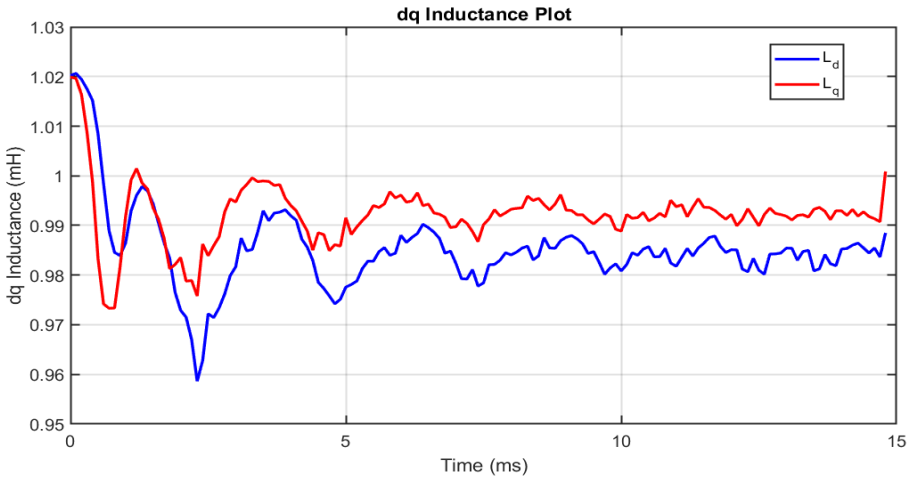

Fig. 12: Variation of D-Axis and Q-Axis Inductances with Time.

Figure 13 presents the d–q axis flux linkages of the designed axial flux PMSM during transient simulation. The blue curve represents the d-axis flux linkage (Φ_d), while the red curve corresponds to the q-axis flux linkage (Φ_q). At the beginning of the simulation, both flux linkages exhibit small oscillations due to the transient start-up response and rotor position alignment. As the motor reaches steady-state, the flux linkages stabilize, maintaining nearly constant values throughout the simulation period. The Φ_d component stabilizes around 0.05 Wb, whereas Φ_q settles near –0.04 Wb, reflecting proper orthogonal decoupling of the d–q axes under field-oriented control conditions. The steady and smooth flux linkage characteristics indicate effective magnetization of the rotor magnets and a well-designed magnetic circuit, which minimizes cross-coupling effects and ensures stable electromagnetic torque generation.

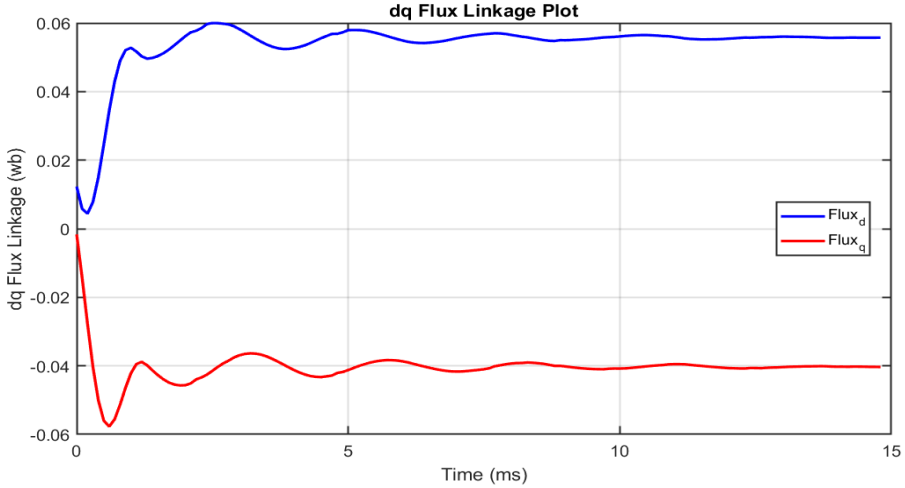

Fig. 13: Flux Linkage in the D-Q Reference Frame.

Figure 14 presents the d-q axis current components during motor operation, as extracted from ANSYS Maxwell 3D transient simulation. The direct-axis current i_d (red waveform) exhibits a rapid rise from near-zero values to approximately 50 A within the initial 15ms, subsequently stabilizing at approximately 40–45 A during steady-state operation. The quadrature-axis current i_q (blue waveform) demonstrates a complementary behavior, initially rising to approximately -60 A before settling to a steady-state magnitude of approximately -45 A. The balanced current distribution across the d-q reference frame confirms the effectiveness of the field-oriented control strategy and validates the motor's ability to maintain consistent electromagnetic performance under the specified operating conditions.

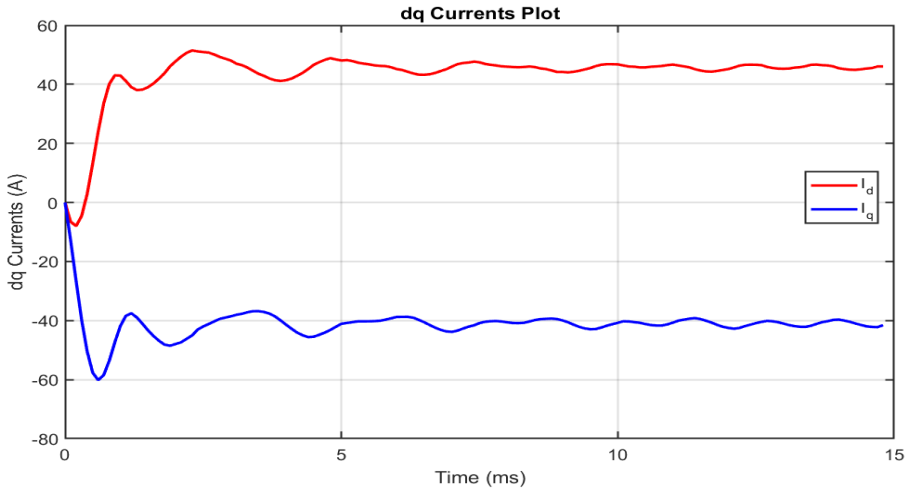

Fig. 14: Current in the D-Q Reference Frame.

The torque response of the AF-PMSM is presented in Figure 15, reveals an initial transient phase (0–15ms seconds) with rapid fluctuations reaching a peak of approximately 6.5 Nm, followed by stabilization to a steady-state mean torque of approximately 3.5 to 4 Nm with periodic ripple. The controlled torque ripple magnitude, evidenced by the oscillations around the mean value, is characteristic of well-designed ferrite-based permanent magnet machines and indicates effective electromagnetic force balance. The steady-state torque demonstrates the motor's capability to sustain load operation reliably, validating the motor design, material selection, and control implementation for the specified duty cycle.

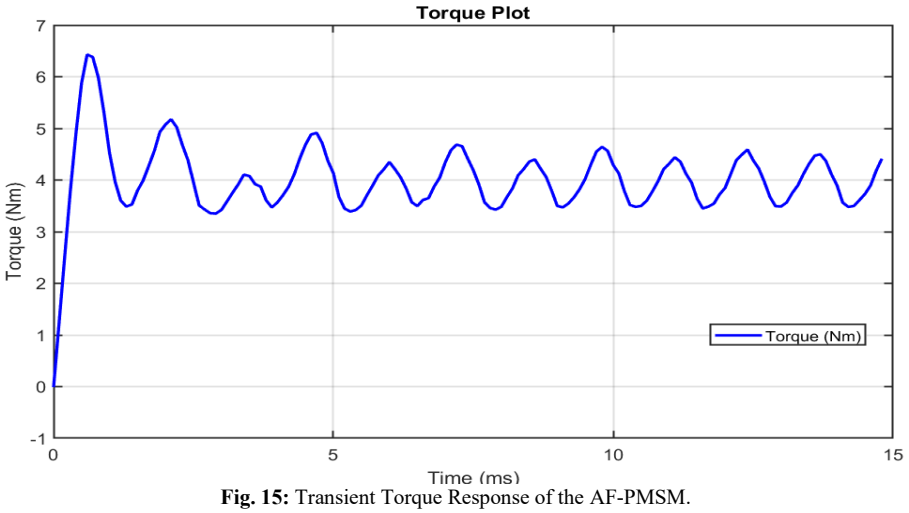

Fig. 15: Transient Torque Response of the AF-PMSM.

3.3. Analytical calculation

From the Simulation Results, $i_d = 40A$ & $i_q = -60A$
L_d =0.0875 mH= 0.0000875H
L_q =0.0975 mH = 0.0000975H

q-axis flux $\lambda_q = L_q i_q$ (14)

$\lambda_q = -0.005850$ Wb

d-axis flux $\lambda_d = L_d i_d + \lambda_m$ (15)

No: of poles, p=12
Electromagnetic Torque

$$T_e = \frac{3}{2}\frac{p}{2}(L_d - L_q) i_d i_q + \frac{3}{2}\frac{p}{2}\lambda_m i_q \quad (16)$$

$T_e = 6.1$Nm

Output Power $P_{out} = T_e * \omega = T_e * \frac{2\pi N}{60}$ (17)

$P_{out} = 2.5$ kW

The simulation results of transient analysis, demonstrate that the axial flux PMSM equipped with ferrite permanent magnets achieves a rated electromagnetic torque of 6.1 Nm and an output power of approximately 2.5 kW at 3900 rpm. These findings validate the analytical performance predictions and underscore the viability of ferrite-based magnets as a cost-effective alternative for electric vehicle propulsion systems. To comprehensively evaluate how material composition influences axial flux PMSM performance, three focused parametric studies were conducted: (i) systematic variation of core materials to assess magnetic and mechanical properties, (ii) comparative analysis of permanent magnet grades to determine optimal magnetic flux density and coercivity characteristics, and (iii) investigation of conductor material alternatives to optimize electrical conductivity and thermal performance.

3.4. Influence of core materials in AF-PMSM

To systematically assess the influence of alternative core materials in AF-PMSM design, high-performance magnet steels (10JNEX900, Hiperco50), a representative soft magnetic composite (Hoganas1000 5P@800Mpa), and additional alloys (Permenorm5000, Metglas-2605S3A, Nano Powder Composite) were evaluated. For baseline comparison, all other parameters including permanent magnet type (Ferrite), winding conductor (Copper_75C), and motor geometry were held constant. Table IV compiles the comparative results for iron-core loss, total loss, efficiency, and net component mass.

Table 4: Specification and Geometrical Parameters

Core material grade	Iron-core Loss (KW)	Total Loss (KW)	Efficiency %	Net weight (Kg)
10JNEX900	0.0034335	1.5538	61.67	2.40887
Hiperco50	0.0067114	1.5609	61.562	2.55938
Permenorm5000	0.001	1.5495	61.736	2.59116
Metglas-2605S3A	0.0012	1.5499	61.730	0.612463
Nano Powder Composite	0.00411	1.5548	61.655	0.612463
Hoganas1000 5P@800MPa	0.012476	1.587	61.170	0.612463

These results demonstrate a narrow efficiency range (61.17–61.74%) and minimal total loss variation for all core material grades, affirming that with Ferrite magnet the combined impact of core material selection is modest relative to winding and magnet losses. Notably, soft magnetic composites and advanced alloys (Hoganas1000 5P @800MPa, Permenorm5000, Metglas-2605S3A, Nano Powder Composite) achieve nominal core losses yet do not manifest meaningful efficiency gains due to the operational dominance of copper_75C and magnet losses, a result corroborated by recent studies [25] [26]. To further elucidate core material impact, the motor was simulated with NdFeB35 magnet and the same set of core materials. Performance measures are presented in Table V.

Table 5: Specification and Geometrical Parameters

Core material grade	Iron-core Loss (KW)	Total Loss (KW)	Efficiency %	Net weight (Kg)
10JNEX900	0.030262	0.47824	83.94	2.54323
Hiperco50	0.078755	0.41	85.911	2.69374
Permenorm5000	0.04355	0.53855	82.277	2.72551
Metglas-2605S3A	0.07541	0.63343	79.787	0.746821
Nano Powder Composite	0.08434	0.85226	74.578	0.746821
Hoganas 1000 5P@800MPa	0.10627	0.53011	82.506	2.55043

Compared to the Ferrite magnet, switching to the high-energy NdFeB magnet yields substantial efficiency variation (74.58–85.91%) and much greater sensitivity to iron-core loss. Core materials with minimal loss, such as Hiperco50, markedly improve total motor efficiency, validating the importance of low-loss alloys and composites in rare-earth magnet systems.

3.5. Influence of permanent magnet materials in AF-PMSM

The performance effects of various permanent magnet materials including Alnico5, SmCo24, and advanced NdFeB (N55) were assessed with Hiperco50 and copper_75C winding. Results are tabulated in Table VI.

Table 6: Specification and Geometrical Parameters

Permanent Magnet material	Iron-core Loss (KW)	Total Loss (KW)	Efficiency %	Net weight (Kg)
Alnico5	0.02188	0.8895	73.75	2.68836
SmCo24	0.053648	0.58742	80.974	2.74209
N55	0.090254	0.36726	87.192	2.69911

N55 (Advanced NdFeB) magnet delivers decisively higher efficiency (87.19%) and lower total loss compared to Alnico5 and SmCo24, confirming theoretical expectations associated with its higher energy product and magnetic flux density. SmCo24 offers thermal resilience and moderate performance enhancement but is outperformed by N55 in terms of peak motor efficiency.

3.6. Influence of conductor materials in AF-PMSM

The motor was simulated with Hiperco50, N55 magnet, and various conducting materials. The performance parameters are shown Table VII.

Table 7: Specification and Geometrical Parameters

Conductor	Armature Copper Loss (KW)	Total Loss (KW)	Efficiency %	Net weight (Kg)
Silver, pure (Ag)	0.20764	0.33986	88.033	2.76151
Gold, pure (Au)	0.28471	0.41693	85.708	3.10726
Aluminium (Al)	0.33458	0. 4668	84.2685	2.45535
Copper (Cu)	0.22537	0.35759	87.48	2.7004

Silver provides the highest efficiency (88.03%) and lowest total loss, marginally outperforming conventional copper winding despite its heavier mass. Gold and aluminium manifest efficiency penalties due to relatively elevated resistivity and loss, making them less favorable for performance-critical applications.

3.7. Inference

These results demonstrate that, in AF-PMSM design, the influence of core material selection becomes substantial when paired with high-flux-density rare-earth magnets, such as NdFeB, with efficiency spanning 74.58–85.91% and total losses ranging 0.41–0.85 kW. Hiperco50, with its superior magnetic properties and negligible core loss, yields the highest efficiency, emphasizing the necessity of low-loss magnet steels for elevated performance. The transition to advanced NdFeB magnets (N55) further amplifies efficiency (up to 87.19%), while Alnico5 and SmCo24 lag due to limited magnetic strength. On the conductor front, silver marginally surpasses copper in performance, yet carries a weight and cost disadvantages. Gold and aluminium conductors, while offering other material benefits, entail substantial efficiency drawbacks. Ultimately, the data reaffirms the critical role of synergistically optimized core, magnet, and conductor materials in realizing superior AF-PMSM architectures for demanding electric vehicle applications.

4. Conclusion

The comprehensive material assessment demonstrates that AF-PMSM performance is strongly influenced by the synergistic interaction of magnetic, core, and conductor materials. Among the evaluated combinations, the advanced NdFeB (N55) magnets paired with Hiperco 50 cores deliver a peak efficiency of 87.19%, while the use of silver conductors further enhances efficiency to 88.03%, outperforming copper despite the associated increase in weight. Conversely, ferrite–Hiperco 50 configurations offer a cost-effective and lightweight (2.6 kg) alternative, achieving an efficiency of 61.67% and making them suitable for large-scale, economically viable EV production. The N55-based design remains the optimal choice for premium applications where maximum efficiency justifies higher material costs. Importantly, the validated ferrite-based prototype meets the target specifications of 6.1 Nm torque and 2.5 kW at 3900 rpm, confirming the feasibility of ferrite magnets as a supply-secure solution for EV traction motors without compromising essential performance requirements.

References

[1] L. R. Devi, S. Sreekumar, R. Bhakar, and S. Padmanaban, "Electric motor modeling, analysis, and design for E-mobility applications: A state of the art," *e-Prime-Advances in Electrical Engineering, Electronics and Energy,* p. 100985, 2025. https://doi.org/10.1016/j.prime.2025.100985.

[2] P. Sankhwar, "Application of permanent magnet synchronous motor for electric vehicle," *Application of Permanent Magnet Synchronous Motor for Electric Vehicle,* vol. 4, no. 2, pp. 1-6, 2024. https://doi.org/10.54105/ijde.A8028.04020824.

[3] S. Simizu, P. R. Ohodnicki, and M. E. McHenry, "Metal amorphous nanocomposite soft magnetic material-enabled high power density, rare earth free rotational machines," *IEEE Transactions on Magnetics,* vol. 54, no. 5, pp. 1-5, 2018. https://doi.org/10.1109/TMAG.2018.2794390.

[4] A. Mahmoudi, N. Abd Rahim, and H. W. Ping, "Axial-flux permanent-magnet motor design for electric vehicle direct drive using sizing equation and finite element analysis," *Progress In Electromagnetics Research,* vol. 122, pp. 467-496, 2012. https://doi.org/10.2528/PIER11090402.

[5] M. M. Elymany *et al.*, "Advanced methodology for maximum torque point tracking of hybrid excitation PMSM for EVs," *Scientific Reports,* vol. 15, no. 1, p. 7707, 2025. https://doi.org/10.1038/s41598-025-92466-y.

[6] A. Parviainen, "Design of axial-flux permanent-magnet low-speed machines and performance comparison between radial-flux and axial-flux machines," 2005.

[7] M. De Oliveira, V. Steffen, and F. Trojan, "Systematic literature review on electric vehicles and multicriteria decision making: Trends, rankings, and future perspectives," *J. Intell. Manag. Decis,* vol. 3, no. 1, pp. 22-41, 2024. https://doi.org/10.56578/jimd030103.

[8] L. s. Vidyapeeth, M. U. Yadav, and J. D. Kumar, "Choosing the Right Drive: In-depth Motor Selection for Electric Vehicle Traction Systems."

[9] D. O'Donnell, S. Bartos, J. Tjong, and N. C. Kar, "Utilization of innovative materials toward permanent magnet synchronous e-motors for traction application: A review," in *2020 2nd International Conference on Smart Power & Internet Energy Systems (SPIES)*, 2020: IEEE, pp. 380-385. https://doi.org/10.1109/SPIES48661.2020.9243017.

[10] R.-f. Liu, X. Ma, J.-c. Cao, S.-x. Niu, and Z.-g. Wu, "Influence of Amorphous and Silicon Steel on Performance of Permanent Magnet Synchronous Motors Used in Steering Pump of Electric Vehicles," *Journal of Magnetics,* vol. 24, no. 2, pp. 335-341, 2019. https://doi.org/10.4283/JMAG.2019.24.2.335.

[11] S. Rani and R. Jayapragash, "Review on electric mobility: trends, challenges and opportunities," *Results in Engineering,* vol. 23, p. 102631, 2024. https://doi.org/10.1016/j.rineng.2024.102631.

[12] M. Fasil, "Design, modelling, and fabrication of a ferrite magnet axial flux in-wheel motor," 2018.

[13] Q. Chen, D. Liang, Y. Liu, and Q. Wang, "Design and multi-object optimisation of axial flux interior PMSM for EV and HEV applications," *The Journal of Engineering,* vol. 2017, no. 13, pp. 2215-2220, 2017. https://doi.org/10.1049/joe.2017.0724.

[14] R. Tsunata, K. Izumiya, M. Takemoto, J. Imai, T. Saito, and T. Ueno, "Designing and prototyping an axial-flux machine using ferrite PM and round wire for traction applications: Comparison with a radial-flux machine using Nd-Fe-B PM and rectangular wire," *IEEE Transactions on Industry Applications,* vol. 60, no. 3, pp. 3934-3949, 2024. https://doi.org/10.1109/TIA.2024.3371959.

[15] M. H. Mohammadi, R. Nasirizarandi, J. Mistry, and A. Balamurali, "Design of Reduced and Rare-Earth-Free PM-assisted SynRMs for Electric Vehicles to Overcome Electromagnetic-Structural Challenges," in *2025 IEEE International Electric Machines & Drives Conference (IEMDC)*, 2025: IEEE, pp. 865-870. https://doi.org/10.1109/IEMDC60492.2025.11061102.

[16] H.-S. Seol, "Advanced 3D Nonlinear Magnetic Equivalent Circuit Model for Overhang-Type WRSM Design," *Electronics,* vol. 14, no. 7, p. 1304, 2025. https://doi.org/10.3390/electronics14071304

[17] Y. Zhou, K. Liu, X. Yang, C. Zeng, and B. Luo, "Simplified analysis model of axial flux permanent magnet synchronous motor," in *2023 26th International Conference on Electrical Machines and Systems (ICEMS)*, 2023: IEEE, pp. 339-343. https://doi.org/10.1109/ICEMS59686.2023.10345203

[18] R. Akinci and M. Polat, "Design and optimization with genetic algorithm of double rotor axial flux permanent magnet synchronous motor (torus type) for electrical vehicles," in *2019 4th International Conference on Power Electronics and their Applications (ICPEA)*, 2019: IEEE, pp. 1-5. https://doi.org/10.1109/ICPEA1.2019.8911175.

[19] K. P. Schneider, S. Simizu, M. E. McHenry, and M. P. de Boer, "Optimization Study of Rare Earth-Free Metal Amorphous Nanocomposite Axial Flux-Switching Permanent Magnet Motor," *Energies,* vol. 18, no. 3, p. 640, 2025. https://doi.org/10.3390/en18030640

[20] [20]B. Ban, A. Kersten, S. Skoog, L. Sjöberg, S. Stipetić, and T. Batra, "Comparative Analysis of Electric Motor Designs: Traditional Steel Laminations vs. Soft Magnetic Composite Materials," in *2024 International Conference on Electrical Machines (ICEM)*, 2024: IEEE, pp. 1-8. https://doi.org/10.1109/ICEM60801.2024.10700236.

[21] [21]A. Shukla and S. Basak, "Impact of Flux Barriers Shape on the Performance of Reduced Rare-Earth Multilayer Interior Permanent Magnet Synchronous Motor," in *IECON 2024-50th Annual Conference of the IEEE Industrial Electronics Society*, 2024: IEEE, pp. 1-6. https://doi.org/10.1109/IECON55916.2024.10905700.

[22] [22]E. M. Hammad, F. E. Abdel-Kader, M. E. Ibrahim, and M. A. Shanab, "Rotor Flux Barrier Design for Torque Improvement in Synchronous Reluctance Motor," in *2024 25th International Middle East Power System Conference (MEPCON)*, 2024: IEEE, pp. 1-6. https://doi.org/10.1109/MEPCON63025.2024.10850139.

[23] [23]R. Chattopadhyay, J. Jung, M. S. Islam, I. Boldea, and I. Husain, "Rare-Earth Free Unity Power Factor Bi-Axial Excitation Synchronous Machine for Traction Applications," *IEEE Transactions on Industry Applications,* vol. 60, no. 4, pp. 5966-5978, 2024. https://doi.org/10.1109/TIA.2024.3379312.

[24] [24]K. Akizuki *et al.*, "Study of Current Third-Order Harmonics Control to Reduce Iron Loss in Permanent Magnet Synchronous Motors," in *2024 IEEE Energy Conversion Congress and Exposition (ECCE)*, 2024: IEEE, pp. 6252-6257. https://doi.org/10.1109/ECCE55643.2024.10861013

[25] [25]I. Shuaibu, E. H. T. Wei, R. Kannan, and Y. A. Samaila, "Advancements in axial flux permanent magnet machines utilizing coreless technology: A systematic review," *Ain Shams Engineering Journal,* vol. 15, no. 12, p. 103091, 2024. https://doi.org/10.1016/j.asej.2024.103091

[26] [26]P. Samanta, S. B. Mitikiri, P. K. Sahay, and V. L. Srinivas, "A comparative review of radial and axial Flux PMSMs: Innovations in topology, design, and control," *Franklin Open,* p. 100341, 2025. https://doi.org/10.1016/j.fraope.2025.100341.